Additional File 1 for

Integrative genomics approach identifies conserved transcriptomic networks in Alzheimer's disease

Samuel Morabito[1,3], Emily Miyoshi[2,3], Neethu Michael[2,3], Vivek Swarup[2,3,*]

* To whom the correspondence should be addressed: Tel: (949)824-3182; Email: vswarup@uci.edu

This PDF includes:
Figs. S1-S12

Table of contents

Supplemental Figures

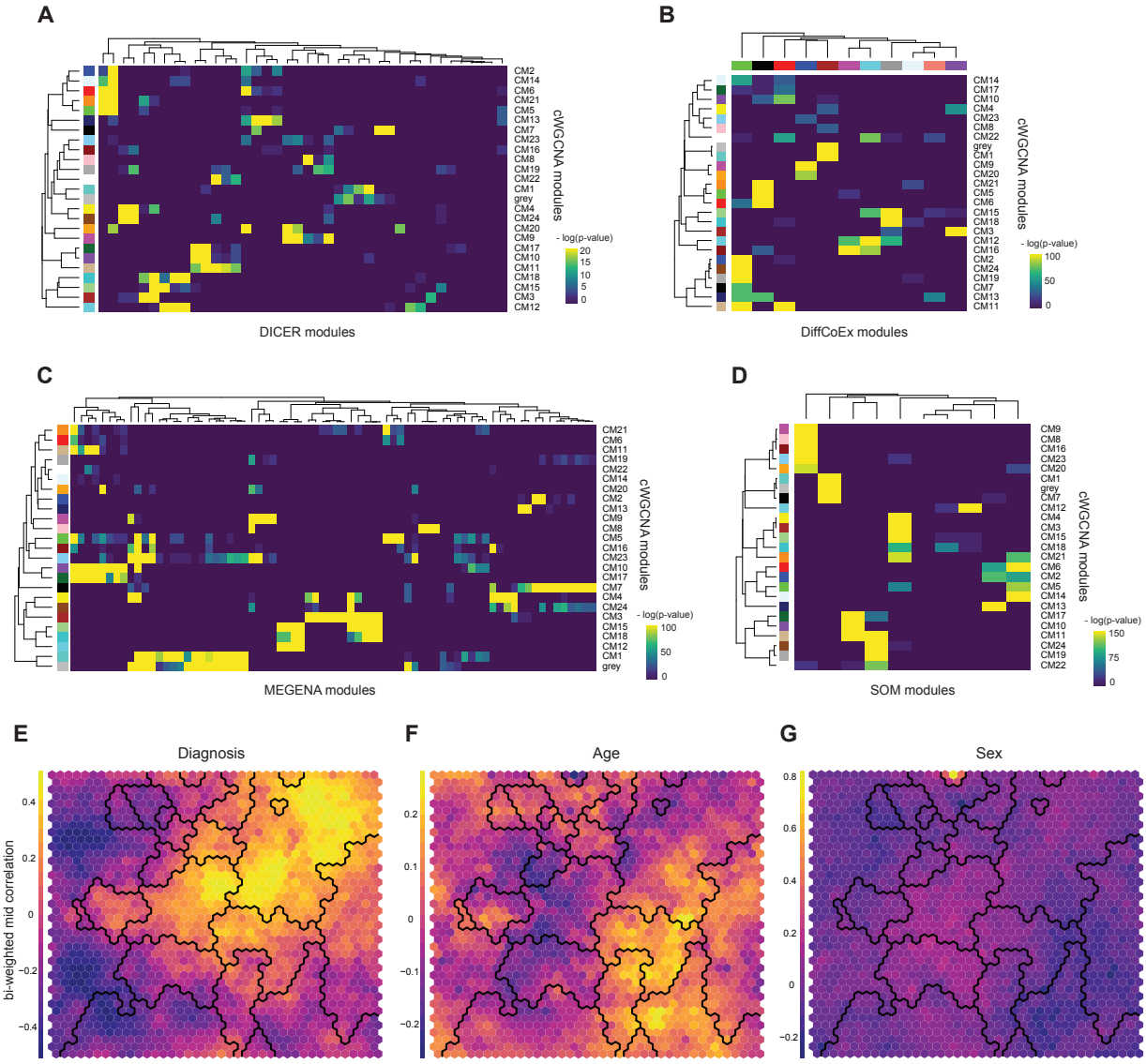

Fig. S1: Comparison of modules from cWGCNA to other methods

(a-d) Heatmaps showing the overlap between gene modules from cWGCNA and gene modules from **(a)** DICER, **(b)** DiffCoEx, **(c)** MEGENA, and **(d)** Self-organizing map (SOM), colored by -log(p-value) from a hypergeometric overlap test. **(e-g)** SOM computed using samples from the Mayo cohort, colored by bi-weighted mid correlation with **(e)** AD Diagnosis, **(f)** age at death, **(g)** and sex.

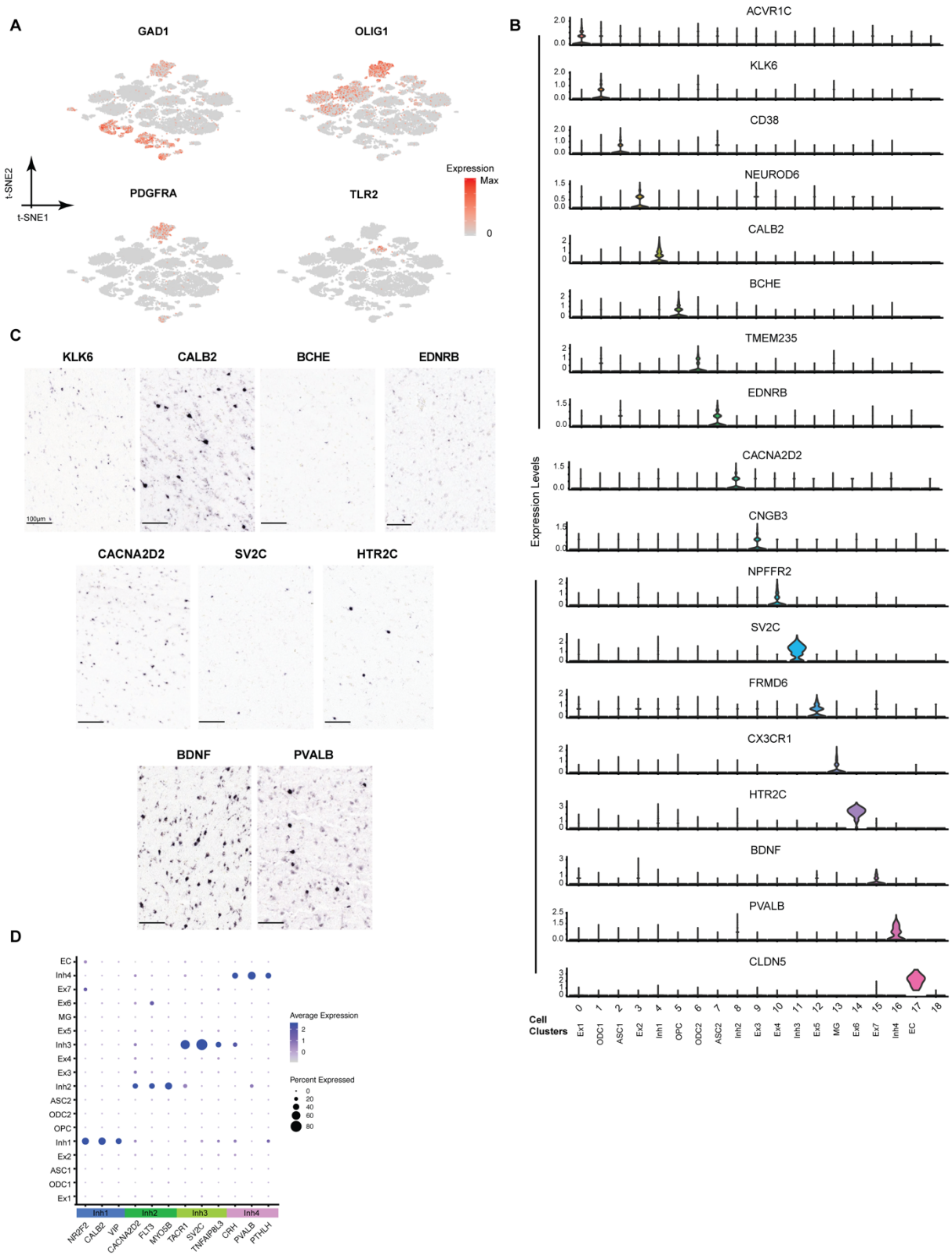
A
GAD1
OLIG1
PDGFRA
TLR2
t-SNE2
t-SNE1
Expression
Max
0
B
ACVR1C
KLK6
CD38
NEUROD6
CALB2
BCHE
TMEM235
EDNRB
CACNA2D2
CNGB3
NPFFR2
SV2C
FRMD6
CX3CR1
HTR2C
BDNF
PVALB
CLDN5
Expression Levels
Cell Clusters
C
KLK6
CALB2
BCHE
EDNRB
100μm
CACNA2D2
SV2C
HTR2C
BDNF
PVALB
D
EC
Inh4
Ex7
Ex6
MG
Ex5
Inh3
Ex4
Ex3
Inh2
ASC2
ODC2
OPC
Inh1
Ex2
ASC1
ODC1
Ex1
Average Expression
Percent Expressed
NR2F2
CALB2
VIP
CACNA2D2
FLT3
MYO5B
TACR1
SV2C
TNFAIP8L3
CRH
PVALB
PTHLH

Fig. S2. Single-cell cluster marker gene expression

(**a**) Marker gene enrichment in cell-type clusters visualized with same t-SNE plot as in Figure3a. **(b)** Violin plots of differentially expressed cell-type markers in each cell-type cluster identified by snRNA-seq. (**c**) RNA ISH of a subset of the differentially expressed cell-type markers in human cortical tissue. Images from the Allen Human Brain Atlas. (**d**) Dot plot showing differentially expressed inhibitory neuronal markers in cell-type clusters. Color denotes average gene expression, while size denotes percent of nuclei expressing the gene.

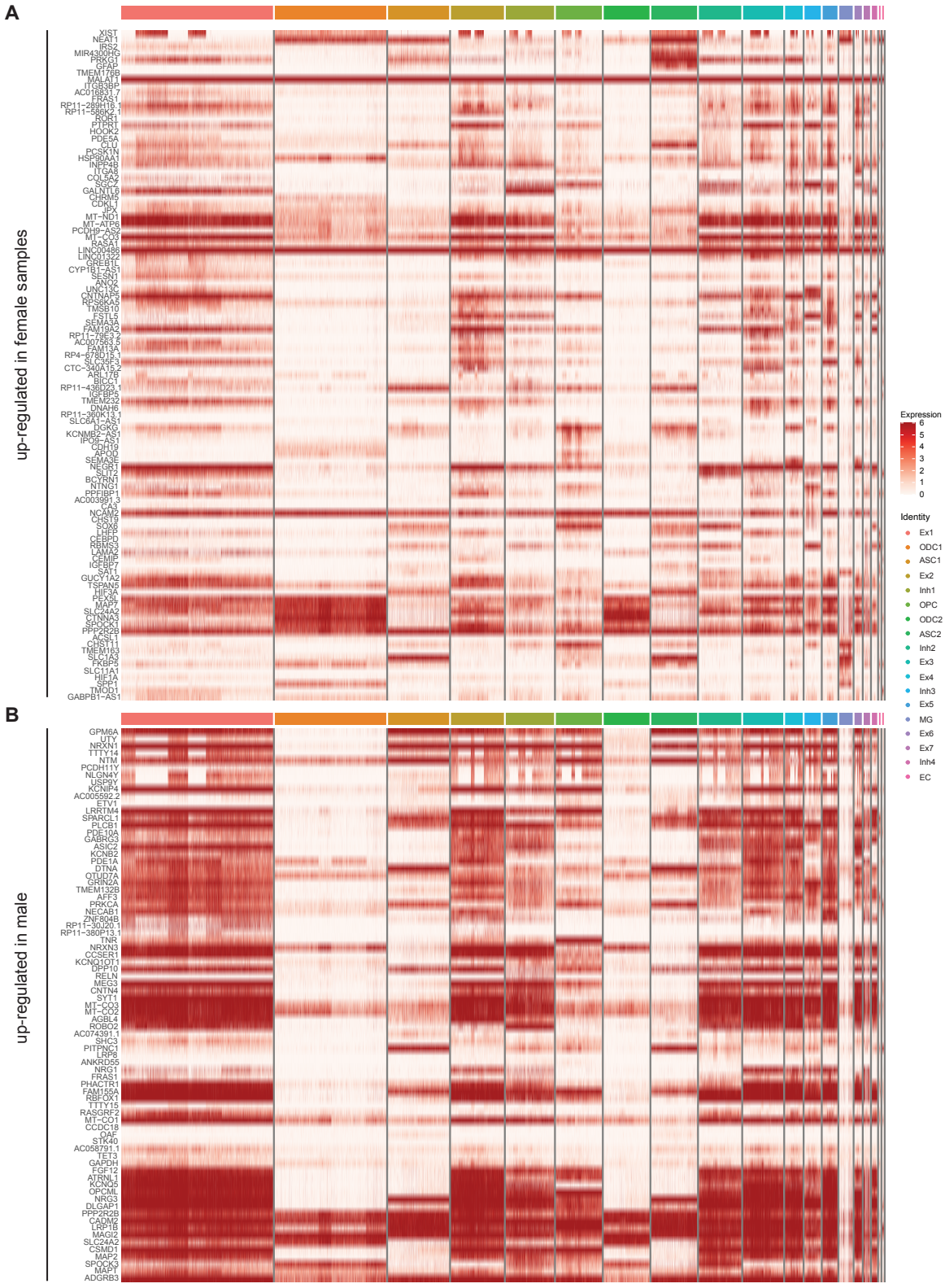
A
up-regulated in female samples
XIST
NEAT1
IRS2
MIR4300HG
PRKG1
GFAP
TMEM176B
MALAT1
ITGB3BP
AC016831.7
FRAS1
RP11-289H16.1
RP11-589K2.1
ROR1
PTPRT
HOOK2
PDE5A
CLU
PCSK1N
HSP90AA1
INPP4B
ITGA8
COL5A2
SOX2
GALNT18
CHRM5
CDK14
IPX
MT-ND1
MT-ATP6
PCDH9-AS2
MT-CO3
RASAT
LINC00486
LINC01322
PDE4DIP
CYP1B1-AS1
SESN1
ANO2
UNC13C
CNTNAP5
RPS6KA5
TMSB10
FSTL5
SEMA3A
FAM19A2
RP11-79E3.2
AC007563.5
FAM13A
RP4-678D13.1
SLC39A13
CTC-340A15.2
ARL17B
BICC1
RP11-438D23.1
IGFBP5
TMEM232
DNAH6
RP11-360K13.1
SLC6A1-AS1
DGKG
KCNMB2-AS1
IP5P-AS1
CDH19
APOD
SEMA3E
NEGR1
SLIT2
BCYRN1
NTNG1
PPFIBP1
AC003991.3
CA3
NCAM2
CHST9
SOX8
LHFP
CEBPD
RBMS3
LAMA2
CEMIP
IGFBP7
SAT1
GUCY1A2
TSPAN5
HIF3A
PEX5L
MAP7
SLC24A2
CTNNA3
SPOCK1
PPP2R2B
ACSL1
CHST11
TMEM163
SLC1A3
FKBP5
SLC11A1
HIF1A
SPP1
TMOD1
GABPB1-AS1
Expression
6
5
4
3
2
1
0
Identity
Ex1
ODC1
ASC1
Ex2
Inh1
OPC
ODC2
ASC2
Inh2
Ex3
Ex4
Inh3
Ex5
MG
Ex6
Ex7
Inh4
EC
B
up-regulated in male
GPM6A
UTY
NRXN1
TTTY14
NTM
PCDH11Y
NLGN4Y
USP9Y
KCNIP4
AC005592.2
ETV1
LRRTM4
SPARCL1
PLCB1
PDE10A
GABRG3
ASIC2
KCNB2
PDE1A
DTNA
OTUD7A
GRIN2A
TMEM132B
AFF3
PRKCA
NECAB1
ZNF804B
RP11-30J20.1
RP11-380P13.1
TNR
NRXN3
CCSER1
KCNQ1OT1
DPP10
RELN
MEG3
CNTN4
SYT1
MT-CO3
MT-CO2
AGBL4
ROBO2
AC074391.1
SHC3
PITPNC1
LRP8
ANKRD55
NRG1
FRAS1
PHACTR1
FAM155A
RBFOX1
TTTY15
RASGRF2
MT-CO1
CCDC18
OAF
STK40
AC056791.1
TET3
GAPDH
FGF12
ATRNL1
KCNC2
OPCML
NRG3
DLGAP1
PPP2R2B
CADM2
LRP1B
MAGI2
SLC24A2
CSMD1
MAP2
SPOCK3
MAPT
ADGRB3

Fig. S3: Differentially expressed genes between sex in snRNA-seq

(a-b) Gene expression heatmaps summarizing differentially expressed genes (DEGs) between cells originating from female and male samples within each cluster. The top 10 genes sorted by average log fold change in female **(a)** and in **(b)** male samples for each cluster are displayed.

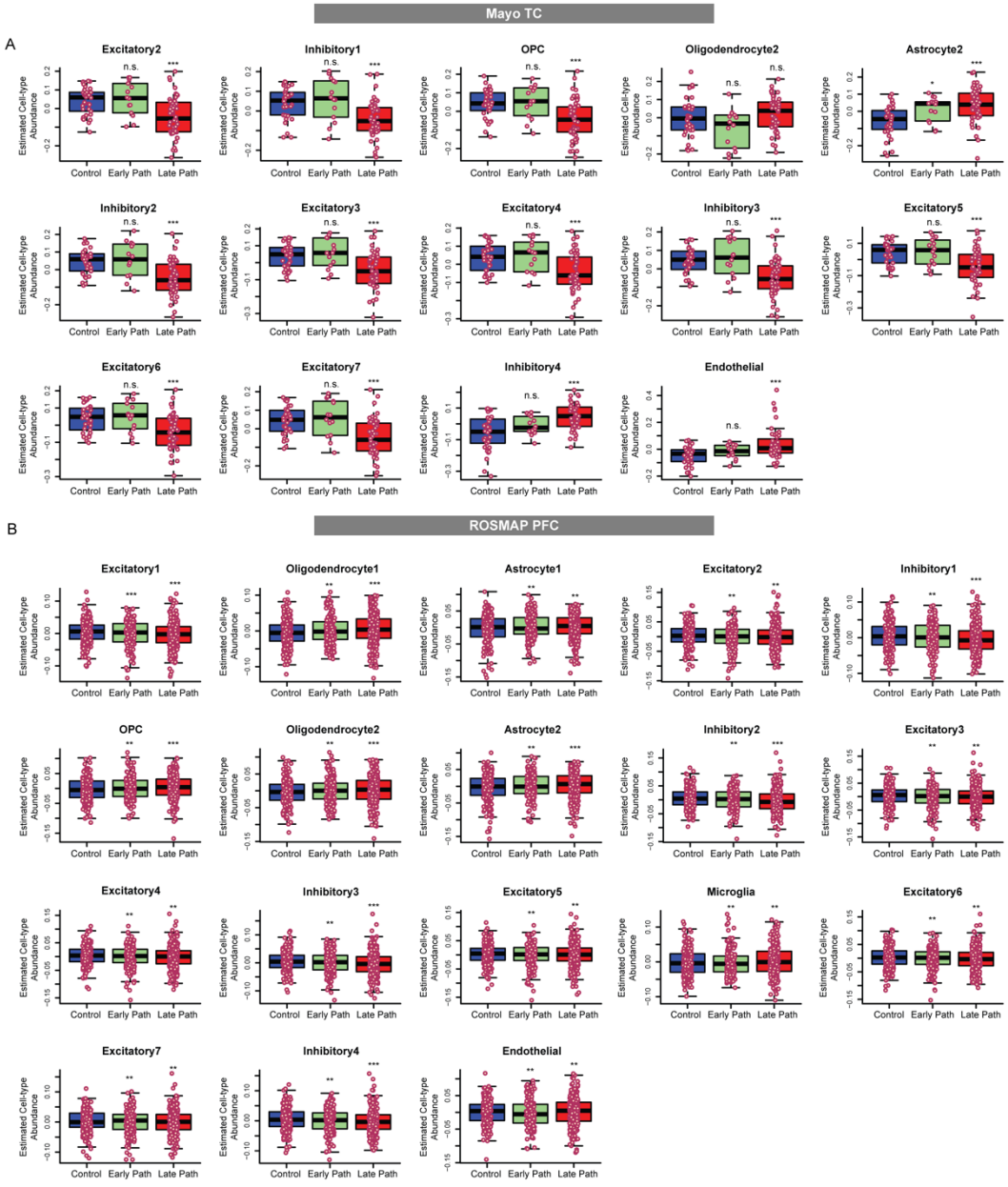

Fig. S4. Cell-type proportion changes in Mayo and ROSMAP datasets

(**a-b**) Boxplots depicting estimated cell-type abundance with pathological state by cell-type cluster in RNA-seq dataset from Mayo TC (**a**) and ROSMAP PFC (**b**).

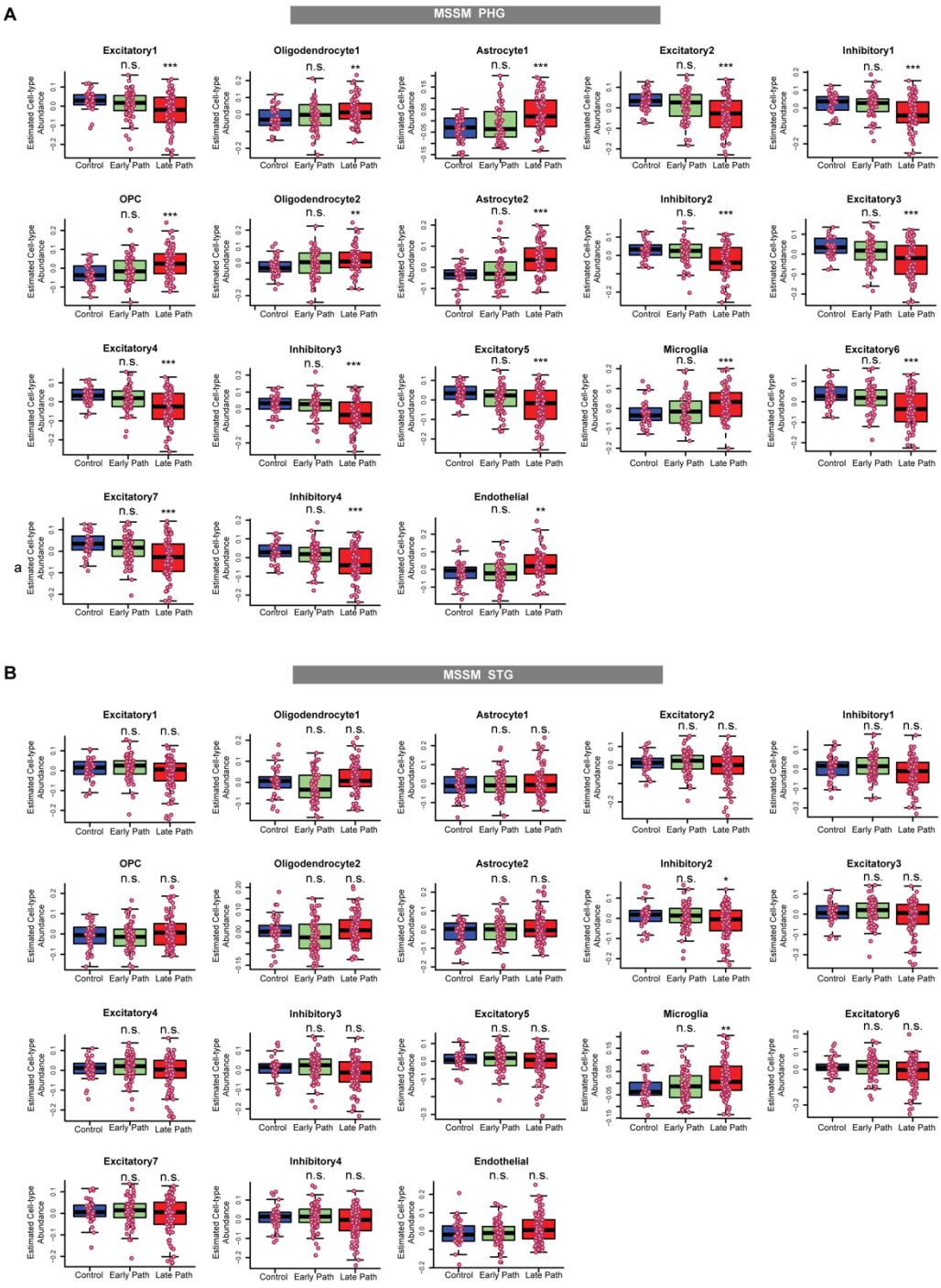

Fig. S5. Cell-type proportion changes in MSSM PHG and STG datasets (**a-b**) Boxplots depicting estimated cell-type abundance with diagnosis by cell-type cluster from RNA-seq dataset from MSSM PHG (**a**) and STG (**b**).

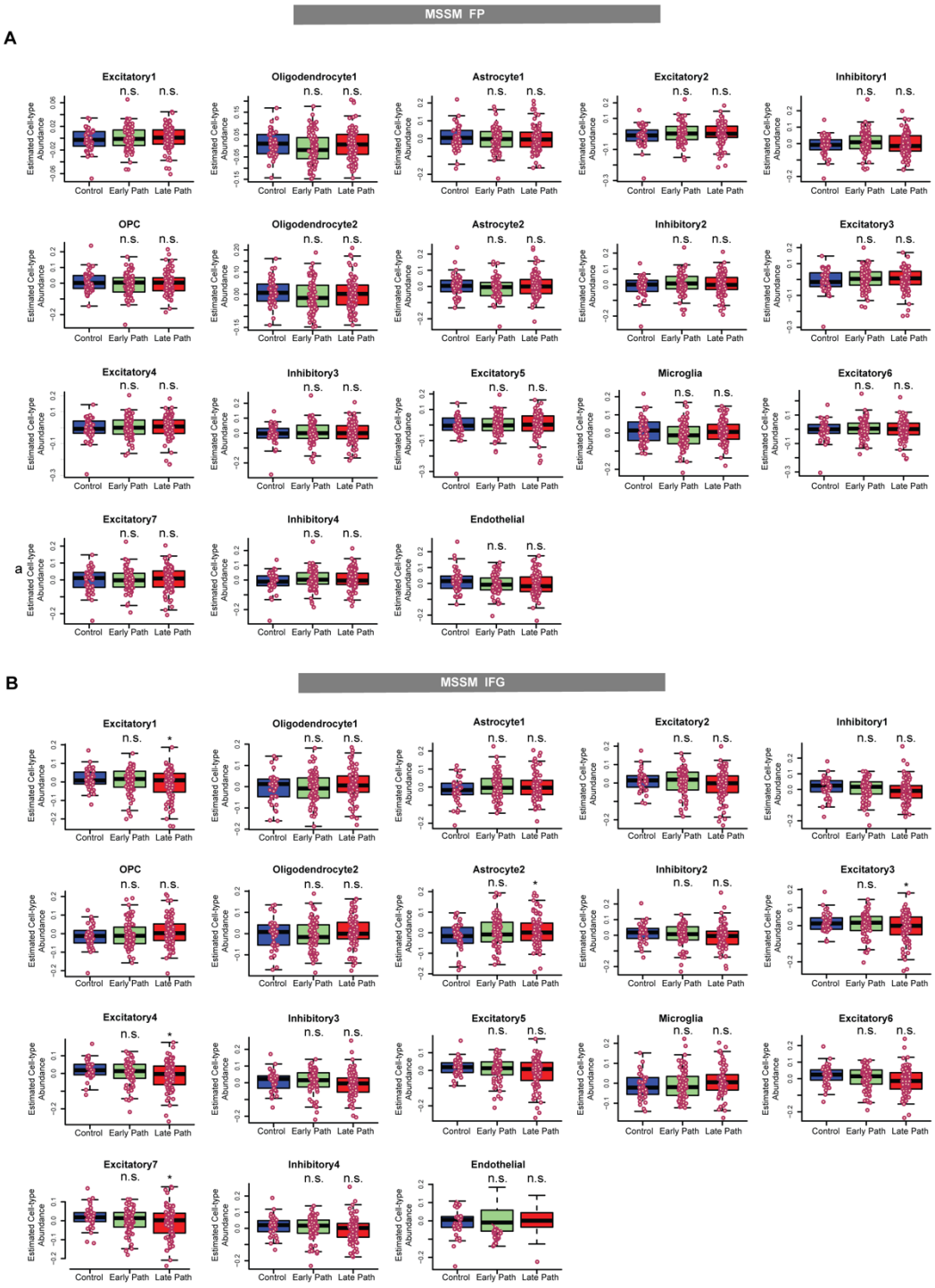

Fig. S6. Cell-type proportion changes in MSSM FP and IFG datasets

(**a-b**) Boxplots depicting estimated cell-type abundance with diagnosis by cell-type cluster from RNA-seq dataset from MSSM FP (**a**) and IFG (**b**).

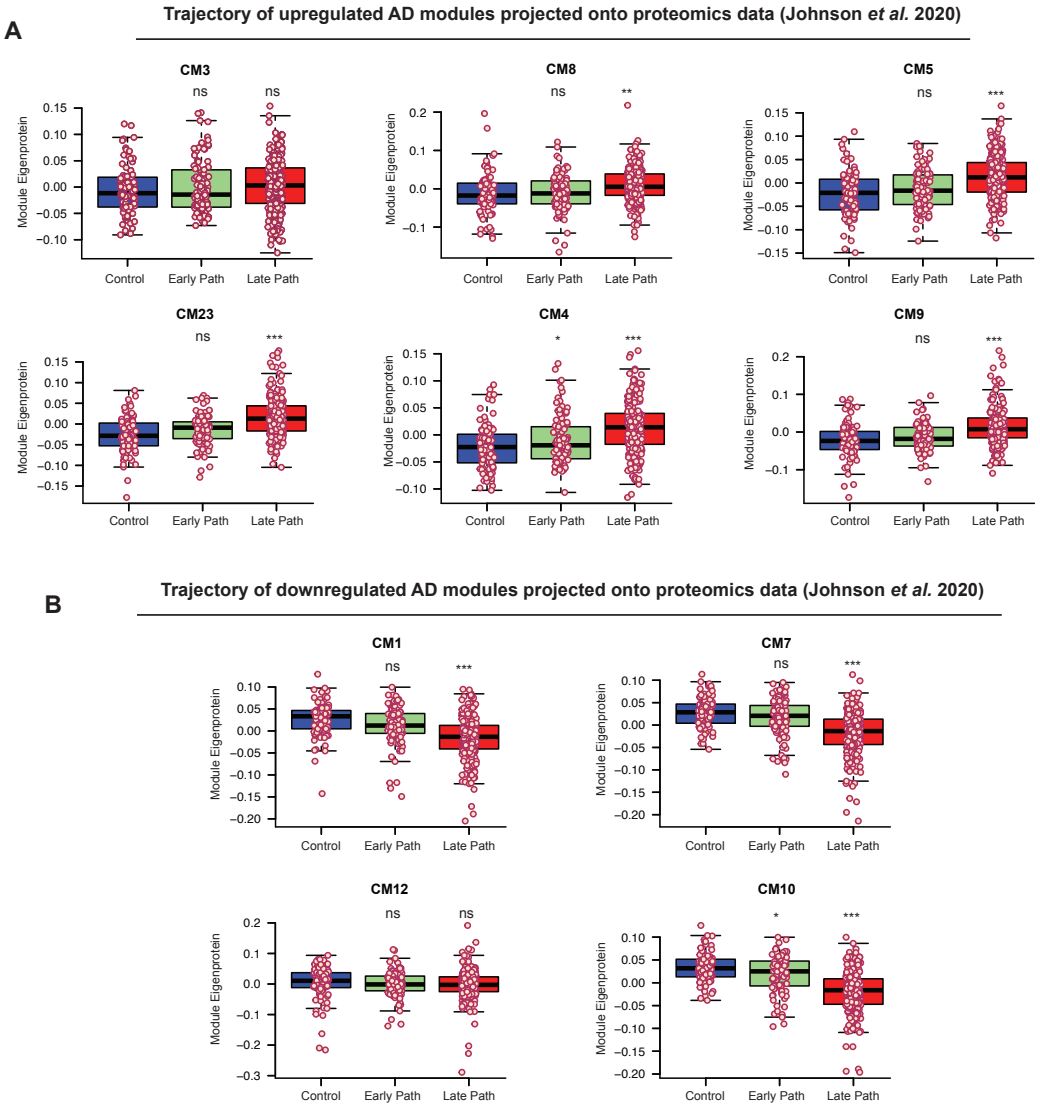

Fig. S7: Trajectory of AD modules projected onto proteomic data

(a-b) Boxplots depicting proteomic module eigenprotein values for modules positively correlated with AD diagnosis **(a)** and for modules negatively correlated with diagnosis **(b)**.

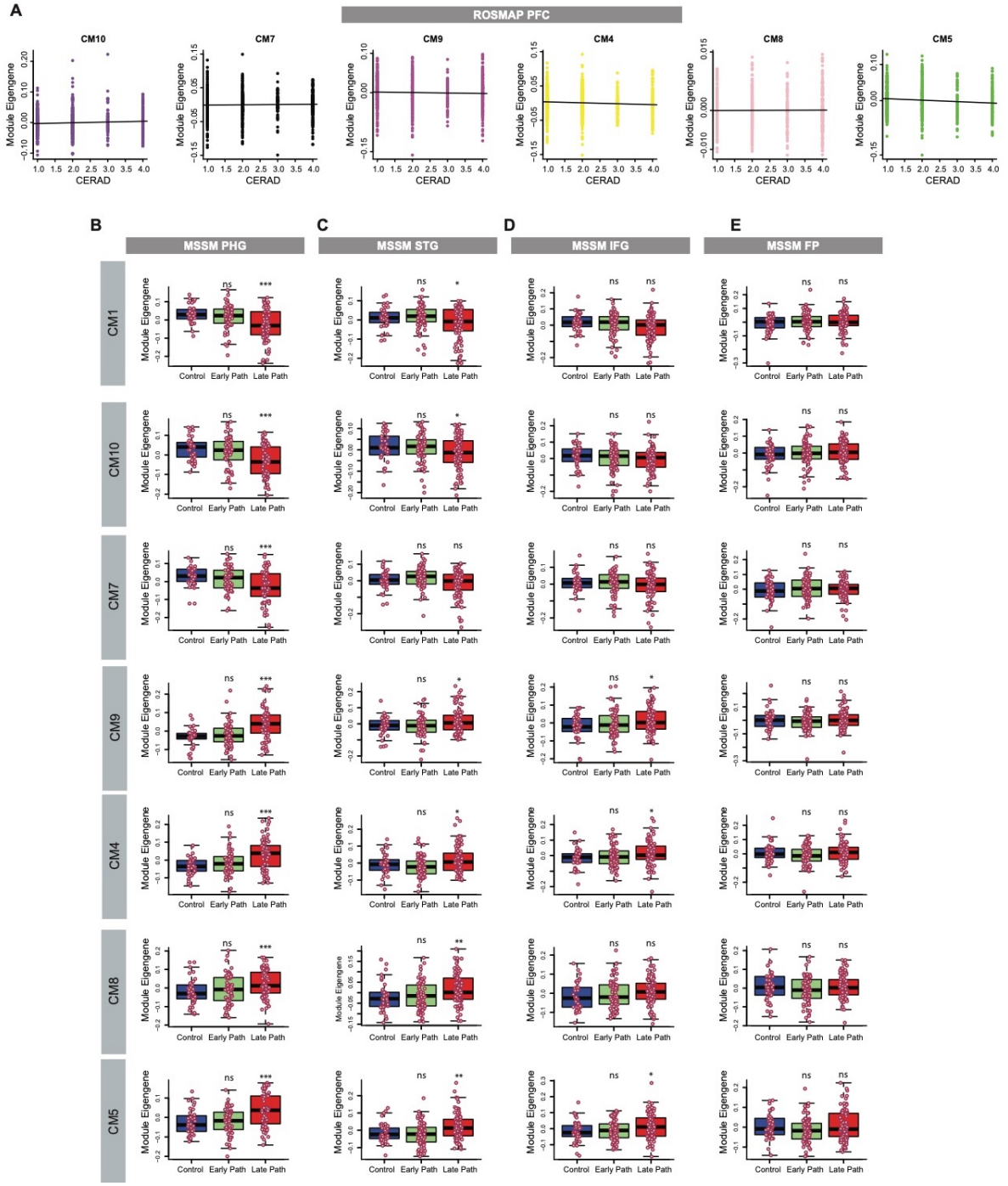

Fig. S8. Consensus WGCNA analysis in ROSMAP and MSSM datasets(**a**) Module eigengene trajectories with CERAD score in ROSMAP PFC dataset. (**b-e**) Boxplot showing module eigengene trajectory with pathological state for neuronal and non-neuronal consensus modules in MSSM PHG (**b**), STG (**c**), IFG **(d)**, and FP **(e)** RNA-seq datasets.

Supplemental Figure 9

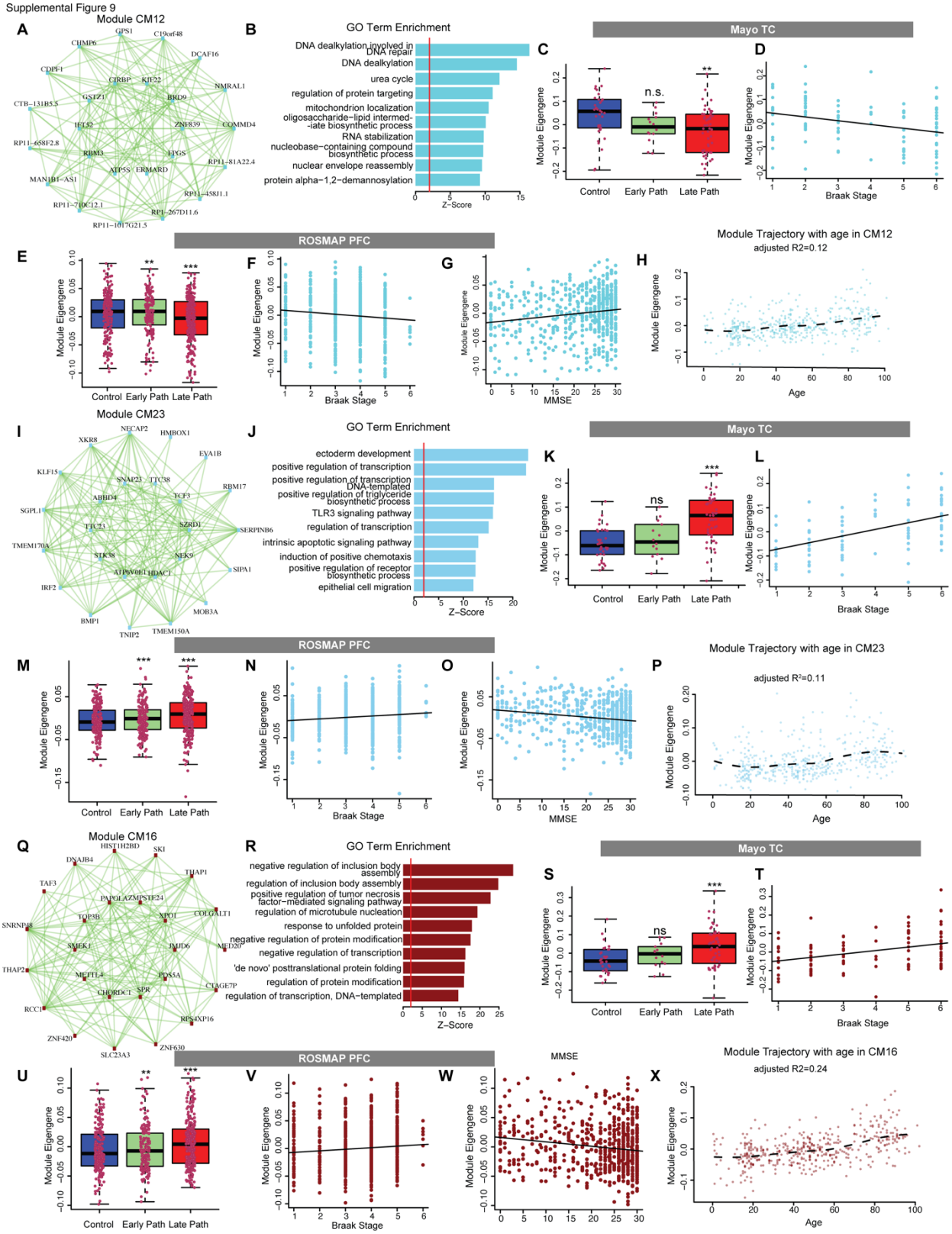

Fig. S9. ME trajectory, pathway analysis and module plots of CM12, CM23 and CM16 modules

(**a-b**) Co-expression plot (**a**) and gene ontology term enrichment (**b**) for neuronal consensus module CM12. **(c-d)** Module eigengene trajectory with pathological state (**c**) and with Braak stage (**d**) for CM12 in Mayo TC dataset. **(e-g)** Module eigengene trajectory with pathological state (**e**), Braak stage (**f**), and MMSE score **(g)** for CM12 in ROSMAP PFC dataset. **(h)** Module eigengene trajectory with age for CM12 in NABEC dataset. (**i-j**) Co-expression plot (**i**) and gene ontology term enrichment (**j**) for non-neuronal consensus module CM23. **(k-l)** Module eigengene trajectory with pathological state (**k**) and with Braak stage (**l**) for CM23 in Mayo TC dataset. **(m-o)** Module eigengene trajectory with pathological state (**m**), Braak stage (**n**), and MMSE score **(o)** for CM23 in ROSMAP PFC dataset. **(p)** Module eigengene trajectory with age for CM23 in NABEC dataset. (**q-r**) Co-expression plot (**q**) and gene ontology term enrichment (**r**) for non-neuronal consensus module CM16. **(s-t)** Module eigengene trajectory with pathological state (**s**) and with Braak stage (**t**) for CM16 in Mayo TC dataset. **(u-w)** Module eigengene trajectory with pathological state (**u**), Braak stage (**v**), and MMSE score **(w)** for CM16 in ROSMAP PFC dataset. **(x)** Module eigengene trajectory with age for CM16 in NABEC dataset.

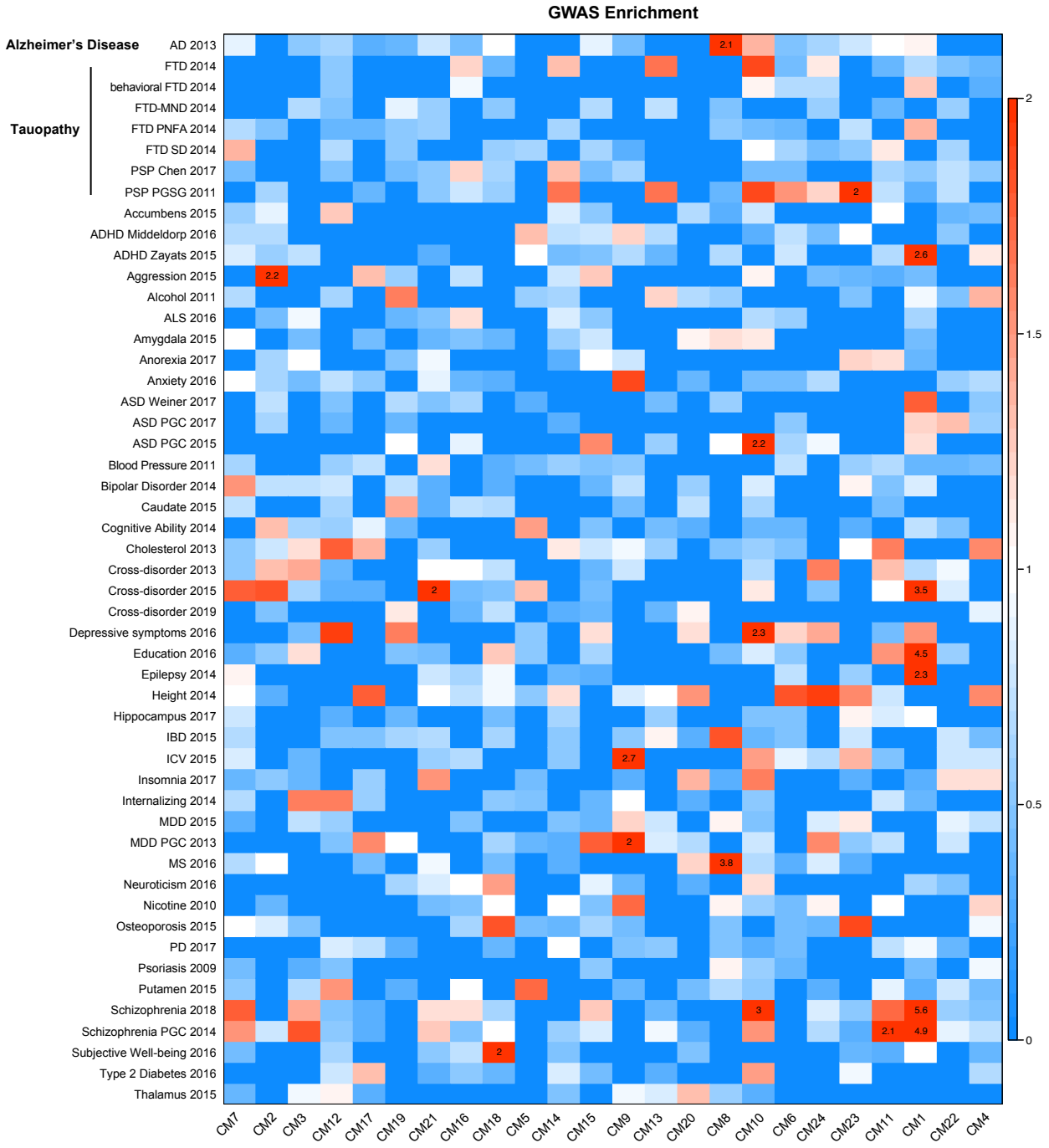

Fig. S10. Enrichment of GWAS hits of other neurodegenerative and neurological disorders

Heatmap of consensus module enrichment of GWAS hits from more than 35 different studies

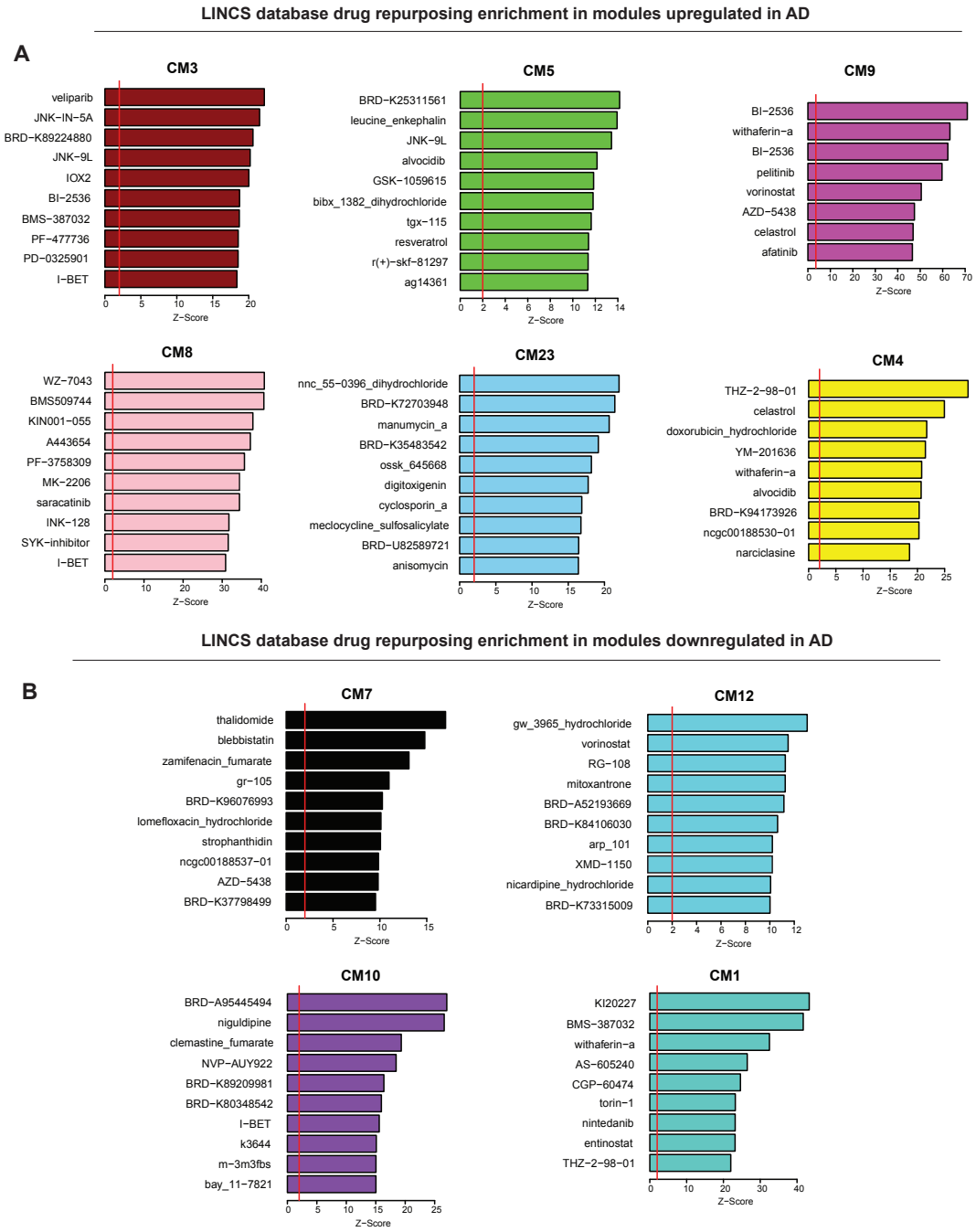

Fig. S11: Potential drug targets for AD consensus modules

(a-b) Bar plots depicting potential drug targets from querying the LINCS database for each module positively correlated with AD diagnosis **(a)** and for each module negatively correlated with AD diagnosis **(b)**.

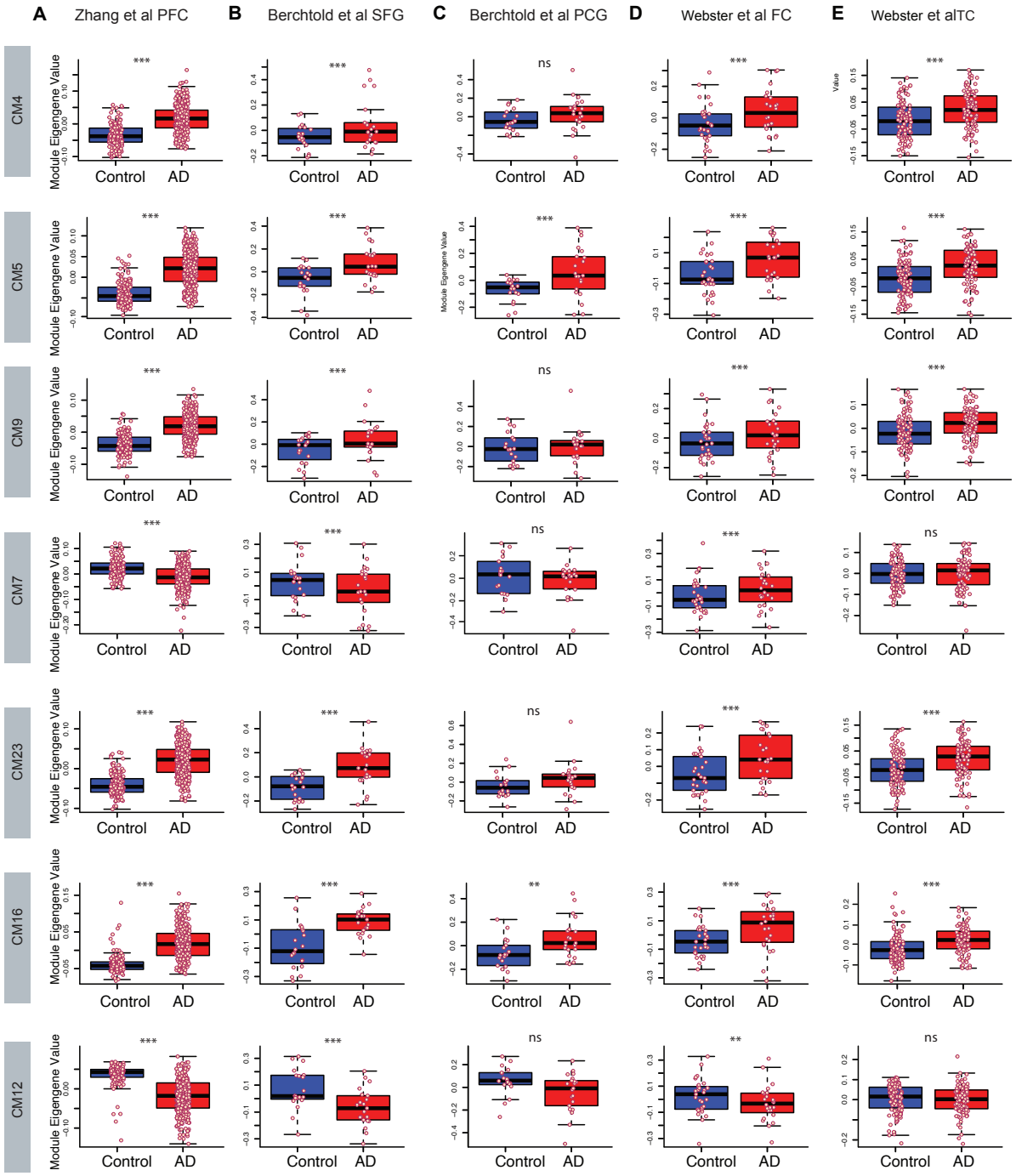

Fig. S12. ME trajectory in published AD datasets

(**a-e**) Boxplots illustrating module eigengene trajectory with diagnosis from RNA-seq dataset from Zhang et al. PFC (61) (**a**), Berchtold et al. SFG (**b**) and PCG (77) (**c**), and Webster et al. FC (78) (**d**) and TC (**e**).